Nuclear Magnetic Resonance Relaxation Studies in Shale

M. E. Ramia & C. A. Martín

Applied Magnetic Resonance

ISSN 0937-9347

Appl Magn Reson
DOI 10.1007/s00723-016-0834-0

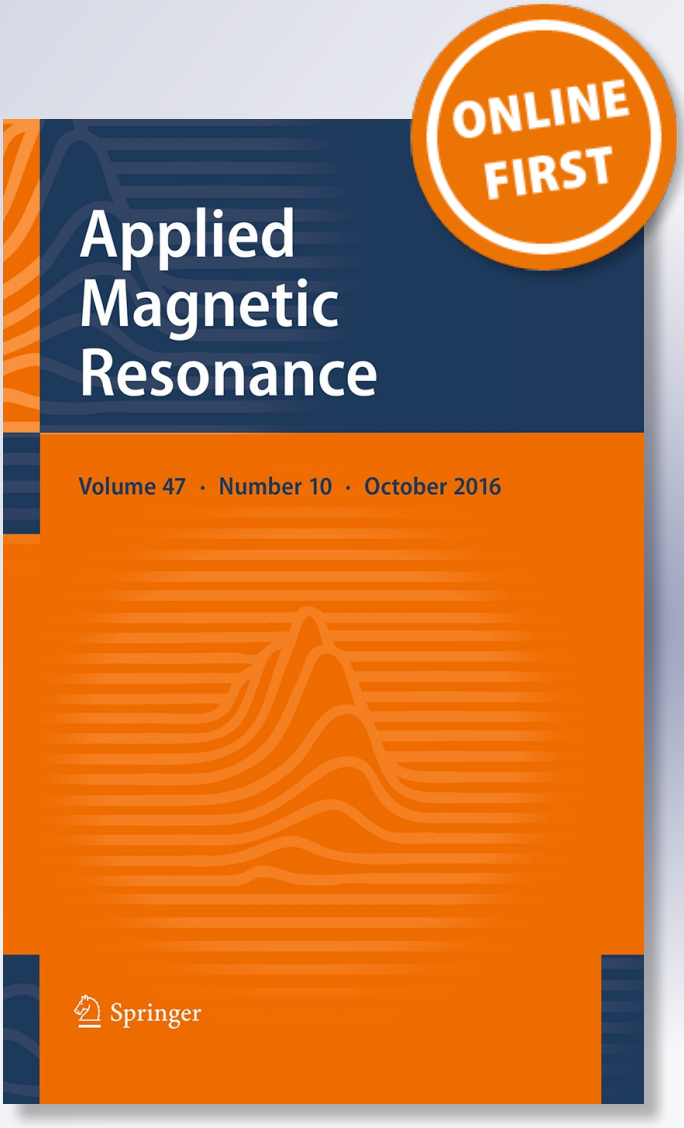

Springer

Appl Magn Reson
DOI 10.1007/s00723-016-0834-0

Applied Magnetic Resonance

ORIGINAL PAPER

Nuclear Magnetic Resonance Relaxation Studies in Shale

M. E. Ramia[1] · **C. A. Martín**[1]

Received: 10 November 2015 / Revised: 18 August 2016

Abstract The present work involves a comprehensive experimental study of proton (^1H) nuclear magnetic resonance (NMR) transversal relaxation in shale. The sample studied belongs to the "Vaca Muerta" formation of the Neuquén basin, Argentina. The results show that the relaxation process is governed by anomalous diffusion processes in micro-pores. These processes result from the combination of interactions between the liquid molecules and the pore walls, whose structure is characterized by both large tortuosity and abundance of paramagnetic impurities, giving rise to local strong time-dependent magnetic field gradients. In addition, a simultaneous experimental method of data fitting is presented which allows processing all the relaxation profiles within a single time domain. Thus, yielding results univocally related to the complete set of relaxation data.

1 Introduction

Experimental electromagnetic techniques, such as nuclear magnetic resonance (NMR), have become nowadays a valuable tool to study porous systems and wettability phenomena related to different materials. Among its many applications, the petroleum well evaluation involves the use of an NMR logging tool, whose main purpose is to provide the proton index, the pore size distribution, the movable an irreducible fluids, the fluids type and content, etc.

The NMR arises from the local interaction of the proton magnetic moments with a magnetic field, composed by both a constant external one plus a local magnetic field from neighboring magnetic dipoles and paramagnetic impurities. In addition, due to

✉ M. E. Ramia
ramia@famaf.unc.edu.ar

[1] Facultad de Matemática Astronomía y Física-Universidad Nacional de Córdoba, 5000 Córdoba, Argentina

Published online: 17 October 2016

the in homogeneities of the tool magnetic field, most of the relevant NMR data come from relaxation measurements and not from spectroscopy. The fluid differentiation is usually achieved by means of diffusion pulse sequences using the magnetic field gradient generated by magnetic field of the tool. This particular setup limits the studies to geological formations, where the tool magnetic field gradient is larger than the internal local field gradients. In addition, for the standard sandstone formations, the penetration of the magnetic field is almost restricted to the invaded region of the rock by the perforation mud, whose conductivity limits the working frequency [1].

The standard relaxation picture, to analyze logging data, taking place in a fully saturated pore, of a given spin I arises from the frequency of visits of one of the fluid molecules to the pore walls, where it undergoes both coupling to the local paramagnetic fields and changes of its dynamics due to wetting phenomena at the pore surface. These wetting effects introduce different changes on the liquid molecules which affect their dynamic favoring semi-rotations, partial adsorption, etc., rather than rapid tumbling as in the pore bulk. As a consequence of the liquid diffusion, the smaller the pore size, the larger is the frequency of interaction of the molecules with the pore wall and the stronger the relaxations effects [2, 3], Fig. 1.

In addition, the logging tools also require low fields, because de electric conductivity of the perforation mud limits the radio-frequency penetration in the rock. Therefore, the convention is to set a magnetic field, such that it generates 2 MHz proton's Larmor frequency, although not limited to higher frequencies for laboratory studies. The picture of a fluid molecule, undergoing Brownian motion and rapid tumbling, inside a filled pore and sensing the surface, taking place in a crust volume surrounding the pore surface, is depicted in Fig. 1.

The most common paramagnetic atoms found in petroleum formations are Fe^{+3} and Mn^{+2} which in small amounts as low as 1 ppm are enough to produce strong relaxation processes [1, 2].

Thus, when a saturated rock is immersed in a homogeneous magnetic field, the fluid protons in the pores respond to an NMR spin-echo T_2 experiment, such that

$$\frac{1}{T_{2P}} = \rho\left(\frac{S}{V}\right)_{\text{pore}} = \frac{\rho}{a}, \tag{1}$$

where $a = V/S$ is the ratio volume to surface of the pore also known as the pore size, and the coefficient ρ is the T_2 surface relaxation strength, or "relaxivity" [4].

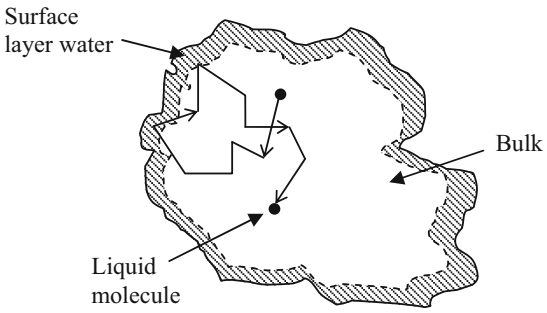

Fig. 1 Motion of a fluid molecule inside a pore

The most convenient way to measure T_2 is by means of the Carr–Purcell–Meiboom–Gill (CPMG) [1, 5] pulse sequence, which yields the total transversal magnetization decay from which the T_2 distribution is obtained, following a discrete non-linear regularized Laplace transformation [6], namely, the signal $S(t; C_i, T_{2i})$ is fitted by

$$S(t; C_i, T_{2i}) = \sum_{i=1}^{n} \left\{ C_i \exp\left(-\frac{t}{T_{2i}}\right) + \alpha |C_{i+1} - C_i| \right\}, \tag{2}$$

with the condition that $C_{n+1} = 0$ and where the coefficients C_i indicate the weight of the decay, provides a mean to measure the pore abundance, whose sizes are characterized by T_{2i}, and α is the regularization coefficient of the fit. The larger α is the more rounded the weight or decay peaks are, introducing continuity to the different changes of the pore sizes abundance [6]. Very important, notice that either C_i or T_{2i} do not depend of each other physically or experimentally.

In addition, to obtain a good *NMR* signal-to-noise ratio, it is required that a reasonable amount of fluids (brine and/or oil) must be contained in the rock pores.

The results obtained from logins of different oil wells, belonging to the geological formations of "Vaca Muerta" basin at Neuquén, and after processed with the standard procedures, by means of Eq. (2), showed unrealistic results. Therefore, a new approach to understand the relaxation process, the theoretical model and the pore structure became necessary.

Since the shale cannot be saturated and/or centrifuged because of its almost zero permeability, which in the case of existing is due to micro-fractures due to the formation diagenesis, implied to work with samples having the preserved natural fluids. In addition, low-frequency measurements, 2 MHz, would have required of large samples which limit the studies, because the measurements involve non-homogeneous radio frequency and constant magnetic fields, due to the experimental setups, which end up introducing a mixture of T_2 and T_1 contributions [7, 8]. Therefore, to overcome these limitations, the studies were performed with small samples and with a much higher resolution 20 MHz spectrometer.

2 Experiment: Sample and Apparatus

2.1 The Sample

Vaca Muerta formation rocks can be described as marine organic rich mudstones with a minor siliciclastic component at the base that gradually passes to limestone towards the formation top and constituted by a succession of marl layers and calcareous claystones with both a high content of total organic carbon, hydrogen index, and paramagnetic salts. This framework composition records the sedimentation and erosion of Triassic–Jurassic volcaniclastic rocks which was exhumed as a result of the Late Jurassic inversion. The shale is characterized by a moderate content of mafic (silicate) volcanic rock sands and plagioclase (family of tectosilicate minerals within the feldspar). The clay and kerogen assemblage is

Fig. 2 Shale grains compared to a millimetric scale

interpreted as the result of a complex set of factors, including source rock, climate, transport, and diagenesis. Post depositional processes produced significant variations in the original compositions, especially the fine-grained deposits [9]. In particular, the sample studied in this work is characterized by a moderate SiO_2, ~ 19 %, content with variable and lesser abundances of both K_2O and Na_2O, and a relatively high proportion NaCl and ferromagnesian paramagnetic elements with kerogen forming the main cement of the sand grains having both low porosity and no permeability. The measurements were performed in sample consisting of grains of few cubic millimeters, as shown in Fig. 2.

2.2 NMR Spectrometer

The NMR equipment used in this work is a Bruker-Minispec-pulsed spectrometer with a working frequency in the range of 20 MHz for proton (^1H) resonance, and the transversal decays to obtain their characteristic times, T_2, distributions were obtained by means of a CPMG pulse sequence with phase alternation, while the total proton content was obtained using a CPMG—T_1-weighted pulse sequence with phase alternation, to separate from the NMR signal of the fluid the Kerogen contribution.

3 Experimental Results

To obtain the "proton index", namely, the amount of protons belonging to preserved fluids in the rock, a comparative measurement of two decays one belonging to the sample, and the other to a brine reference sample were done. In addition, and within the experimental errors, the proton density of per-unit volume of both samples is assumed equal. Figures 3 and 4 show the two decays with $t_e = 0.1$ ms.

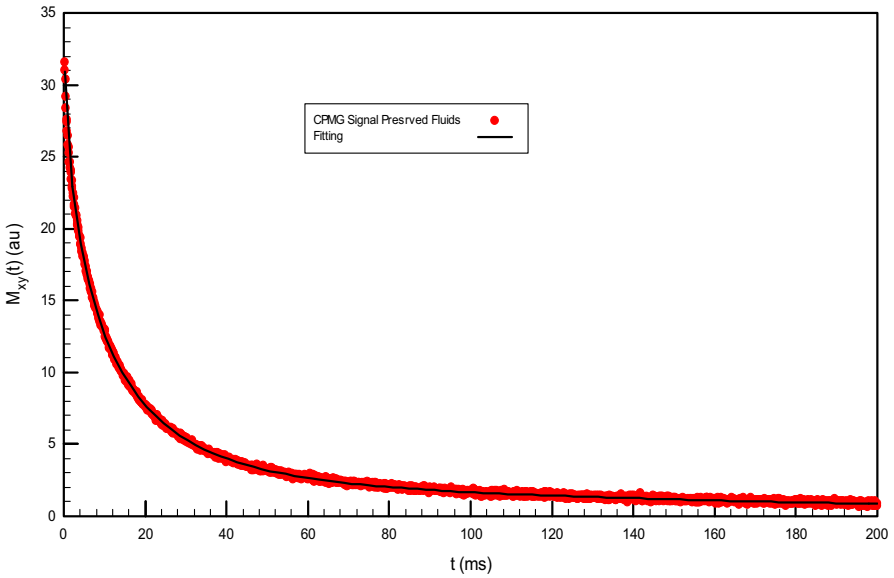

Fig. 3 T_1-weighted T_2 decay curve of the preserved sample fluids in the rock

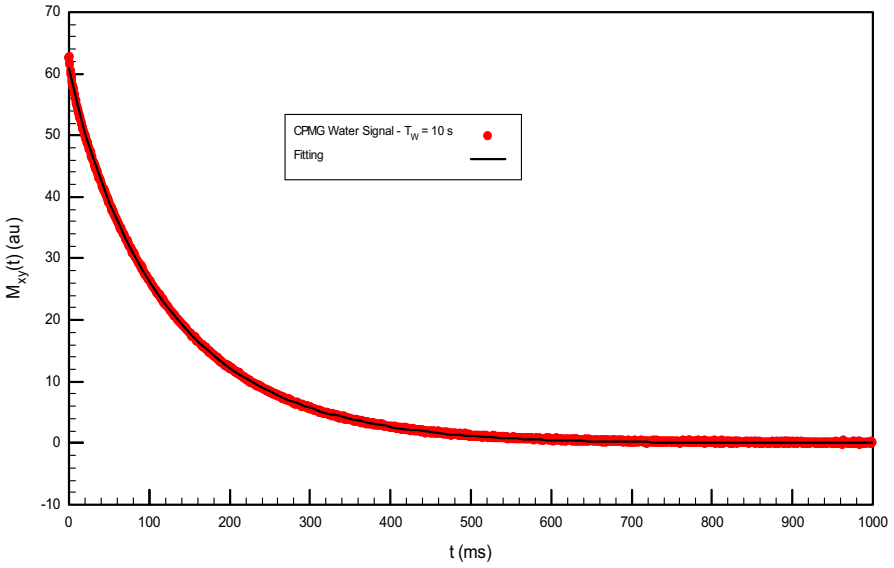

Fig. 4 T_1-weighted T_2 decay curve of the reference brine sample

The black curves in the graphs are the fits by three exponential decays of the experimental points. The percent volume of preserved sample fluids (SF) with respect to the sample volume, or preserved fluids porosity is given by

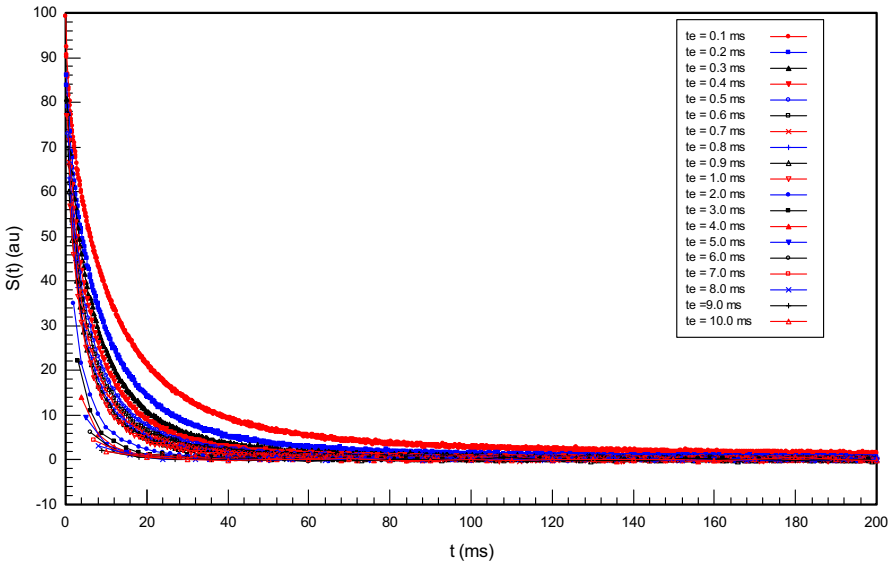

Fig. 5 T_2 decays of the preserved sample fluids in the rock

$$\phi_0 = 100 \frac{\frac{S_{SF}}{V_{SF}}}{\frac{S_W}{V_W}} \cong 17\ \%, \tag{3}$$

where S_W and S_{SF} are the amplitude of the decay curve at $t = 0$ ms. Figure 5 shows transversal relaxation decay data measured with a *CPMG* pulse sequence having different inter pulse times t_e ranging from 0.1 to 10 ms, and Fig. 6 shows essentially the same graph but with an enhanced time axis to depict more clearly the dependence of the relaxation with t_e.

4 The Relaxation Model

It is quite obvious from Figs. 5 and 6 and considering both the spectrometer magnet homogeneity and the sample size that the relaxation is driven by the presence of internal magnetic field gradient in the shale, giving rise to two questions to be answer: What kind of diffusion takes place in the pores? And second, is the diffusion the only present mechanism?

To elucidate these questions, it is convenient to process the experimental data as follows. Figure 7 depicts the normalized, respect to the shortest t_e signal maximum, relaxation decay vs. $t_e^2 t$ in log scale.

To interpret this plot, it must be considered that in the free diffusion regime, the magnetic field gradient G is both time and space independent, and there are no pore wall effects, as for large pores; then, the relaxation signal decays according to the well-known expression [1, 2]

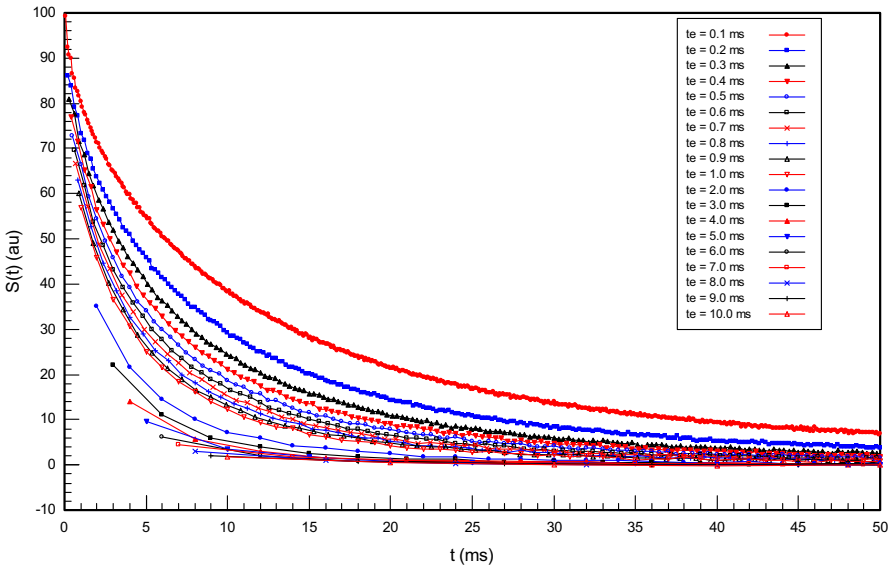

Fig. 6 T_2 decays of the preserved sample fluids in the rock

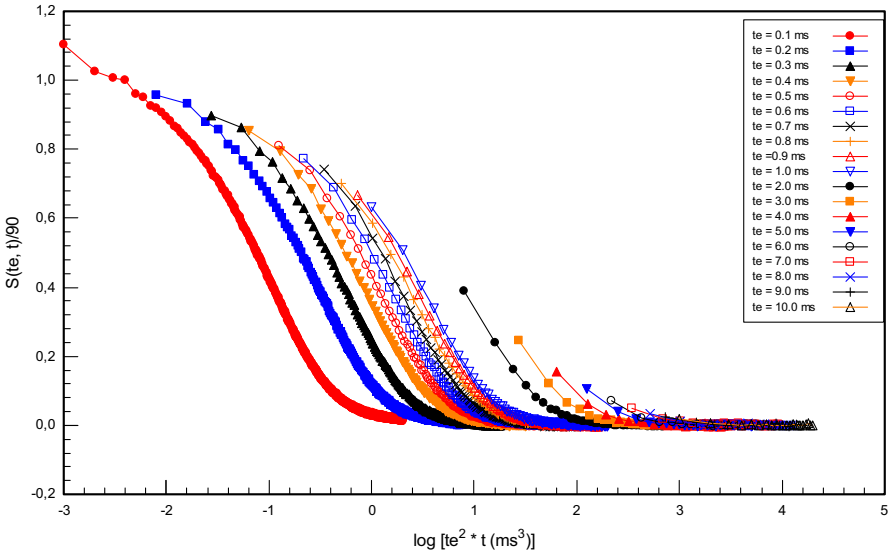

Fig. 7 Normalized relaxation decay signal vs. $t_e^2 t$

$$M(t) = M_0 \exp\left[-\frac{1}{12} D_0 \gamma^2 G^2 t_e^2 t\right] = M_0 \exp\left[-\frac{t}{T_{2D}}\right]. \quad (4)$$

Thus, it should expected that the profiles, at least for the shortest t values, start behaving as a constant function followed by a kink with negative slope at an

approximate value of $t_e^2 t$, such that $(1/12)D_0\gamma^2 G^2 t_e^2 t \cong 0.8$, and an inflection point at $(1/12)D_0\gamma^2 G^2 t_e^2 t = 1$. Obviously, the profiles of Fig. 7 do not exactly behave as previously described. First, at short values of t, the trend is not constant; the data also show a first kink followed by an inflection point at larger values of t. In addition, taking into account that the decay curve corresponding to $t_e = 0.1$ ms contains the maximum information available, and considering that

$$M(t) = M_0 \exp\left[-\frac{t}{T_2}\right] \qquad \frac{1}{T_2} = \frac{1}{T_{2P}} + \frac{1}{T_{2D}} + \ldots \tag{5}$$

Therefore, from Eq. (6)

$$T_2(t) = -\frac{t}{\ln\left(\frac{M(t)}{M_0}\right)}. \tag{6}$$

Which allows to plot the time dependence of T_2^{-1}, as depicted in Fig. 8. Notice that for a T_2^{-1} governed by a single free diffusion Eq. (4) plus a volumetric relaxation Eq. (1), it should behave as a power function or having a profile composed of few plateaus plus a power function. Instead of this behavior, T_2^{-1} shows dependence with t, as shown in Fig. 8. Considering that the relaxation shows three well determined zones, as shown in Fig. 7, the data are well fitted by power functions in each of the regions, such as

$$T_{2i}(t) = at^b; \quad i = S, M, L$$
$$S \Rightarrow t < 2 \text{ ms}; \quad M \Rightarrow 2 \leq t \leq 30 \text{ ms}; \quad L \Rightarrow 30 \text{ ms} < t. \tag{7}$$

Table 1 contains the results of the fits. In addition, Fig. 9 shows a log–log plot of T_2^{-1} vs. t depicting clearly the three time zones.

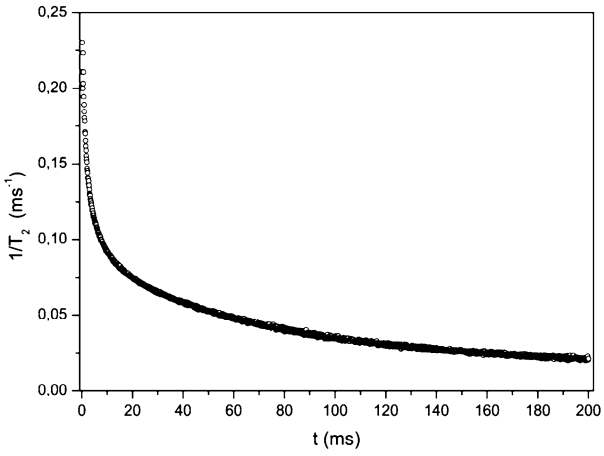

Fig. 8 $1/T_2$ vs. t of the decay with $t_e = 0.1$ ms

Table 1 Fitting parameters of Eq. (8)

i	a	b
S	0.191 ± 0.001	-0.13 ± 0.01
M	0.1846 ± 0.0002	-0.3017 ± 0.0002
L	0.635 ± 0.004	-0.633 ± 0.001

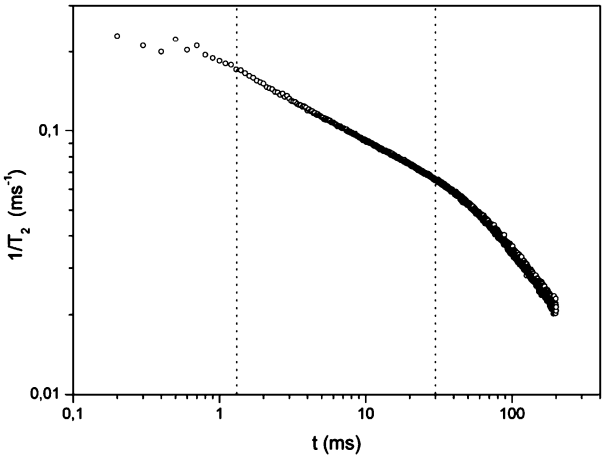

Fig. 9 $\log\left(1/T_2\right)$ vs. $\log(t)$ of the decay with $t_e = 0.1$ ms

It could be argued that $T_2(t)$ shows a restricted diffusion behavior [10], but considering such a case in Eq. (4) D_0 must be replaced by

$$D_{\text{rest}} \cong D_0\left[1 - 0.3144\left(\frac{S}{V}\right)_{\text{pore}}\sqrt{D_0 t_e}\right]. \tag{8}$$

The introduction of this assumption in $T_2(t)$ does not yield satisfactory fitting functions, besides the diffusion coefficient described by Eq. (8) is only valid for perfect reflecting pore walls. Therefore, taking into account all the above observations, it must be concluded that the relaxation taking place in the porous media of this sample is the best described by a modified stretched exponential (MSE) [11, 12] with the magnetic field gradient, G, dependent of time, and

$$M(t) = M_0 \exp\left[-\frac{t}{T_2(t)}\right],$$

with

$$\begin{aligned}\frac{1}{T_2(t)} &= \frac{1}{T_{2P}} + \frac{1}{T_{2S}} = \rho\left(\frac{S}{V}\right)_{\text{pore}} + \beta\left(\frac{D}{12}\gamma^2 G^2\right)^{\beta} t_e^{3\beta-1} \\ &= \frac{\rho}{a} + \beta\left(\frac{D}{12}\gamma^2 G^2\right)^{\beta} t_e^{3\beta-1}.\end{aligned} \tag{9}$$

The MSE model was developed to possess the following characteristics, namely, at very short times and t_e values, it exhibits both a single decay, described by a power law Eq. (7), and a finite initial relaxation rate, while at long times, the function exhibits stretched exponential behavior. The first term of Eq. (9) represents the relaxation rate of all liquid molecules arriving from the pore bulk to the pore surface crust region at the same time, others are released from the crust. On the other hand, the second term of Eq. (9) represents the relaxation of all moving molecules in the crust region undergoing an anomalous diffusion process, namely, diffusion in a zone, where the magnetic field gradient depends of both the position and time. The features described by Eq. (9) have been shown to satisfy the relaxation profiles from pore systems with adsorbing walls and small pore sizes [11].

5 Data Processing

A comprehensive simultaneous data processing requires to yield results univocally related to the whole set of relaxation decay data. Therefore, a simultaneous experimental data fitting which allows processing all the relaxation profiles within a single time domain [13] will provide the desired experimental results. Figure 10 depicts the relaxation decays in a single time domain, the graph also shows the data fitting.

Therefore, based on the previous properties of the relaxation model, the sample is assumed to posses three family of pores characterized by their own relaxation parameters. Consequently, the data are simultaneous fitted by a three exponential decays function, given by

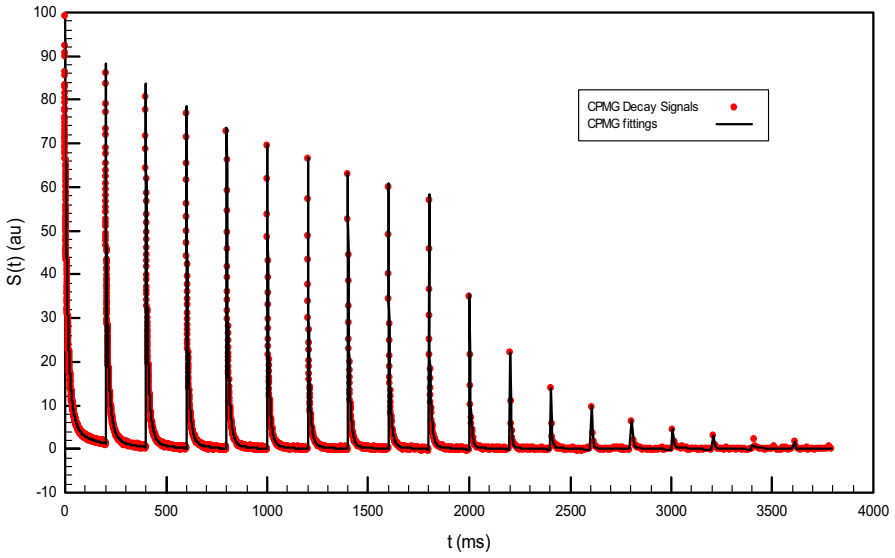

Fig. 10 Relaxation decays arranged in a single time domain; the *black lines* represent the fitting

$$M_i(t) = A_S \exp\left(-\frac{t}{T_{2Si}}\right) + A_M \exp\left(-\frac{t}{T_{2Mi}}\right) + A_L \exp\left(-\frac{t}{T_{2Li}}\right) + A_{0i} \qquad (10)$$
$$0 \le t \le 200 \text{ ms}; \quad 1 \le i \le 19,$$

where each of the relaxation times is given by

$$T_{2Si} = T_{2S}(t_{ei}) = \frac{\frac{a_S}{\rho}}{1 + \frac{a_S}{\rho}\beta_S \left(\frac{D}{12}\gamma^2 G_S^2\right)^{\beta_S} t_{ei}^{3\beta_S - 1}}$$
$$T_{2Mi} = T_{2M}(t_{ei}) = \frac{\frac{a_M}{\rho}}{1 + \frac{a_M}{\rho}\beta_S \left(\frac{D}{12}\gamma^2 G_M^2\right)^{\beta_M} t_{ei}^{3\beta_M - 1}} . \qquad (11)$$
$$T_{2Li} = T_{2L}(t_{ei}) = \frac{\frac{a_L}{\rho}}{1 + \frac{a_L}{\rho}\beta_L \left(\frac{D}{12}\gamma^2 G_L^2\right)^{\beta_L} t_{ei}^{3\beta_L - 1}}$$

Notice that we have introduced three magnetic field gradient, G_S, G_M, and G_M corresponding to each pore sizes. In addition, other parameters, such as the pore abundance, A_S, A_M, A_L, and the exponents $\beta_S, \beta_M, \beta_L$ are also associated with the pore sizes, while both the relaxivity and the diffusion coefficient, ρ, D, are common to all decays. The simultaneous data-processing procedure also provides the values of the relaxation times fitted by Eq. (11), which are shown in Figs. 11, 12, and 13.

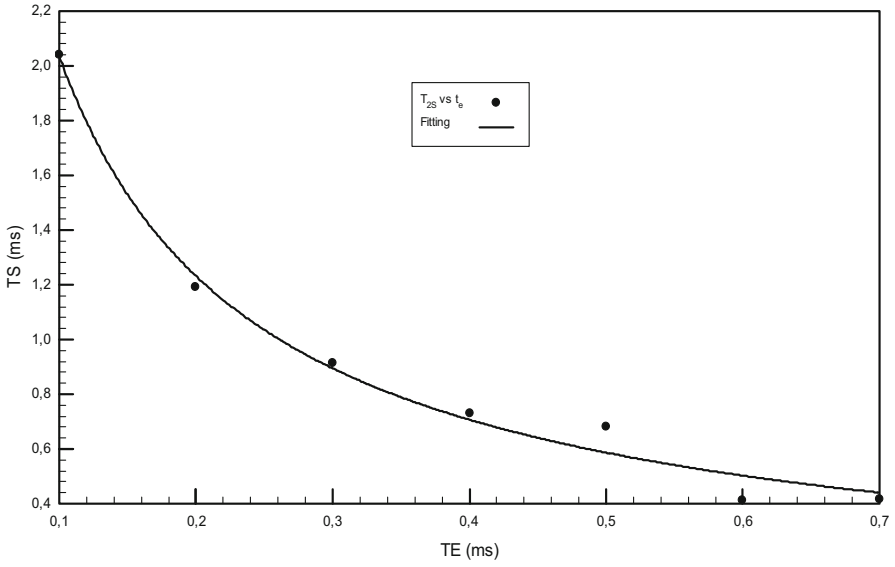

Fig. 11 T_{2S} vs. t_e, the continuous line is the fitting by Eq. (11)

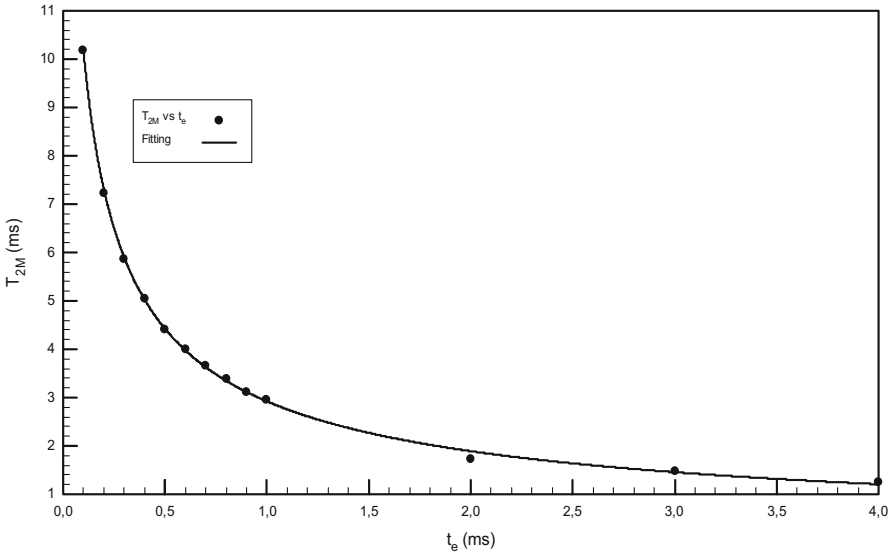

Fig. 12 T_{2M} vs. t_e, the continuous line is the fitting by Eq. (11)

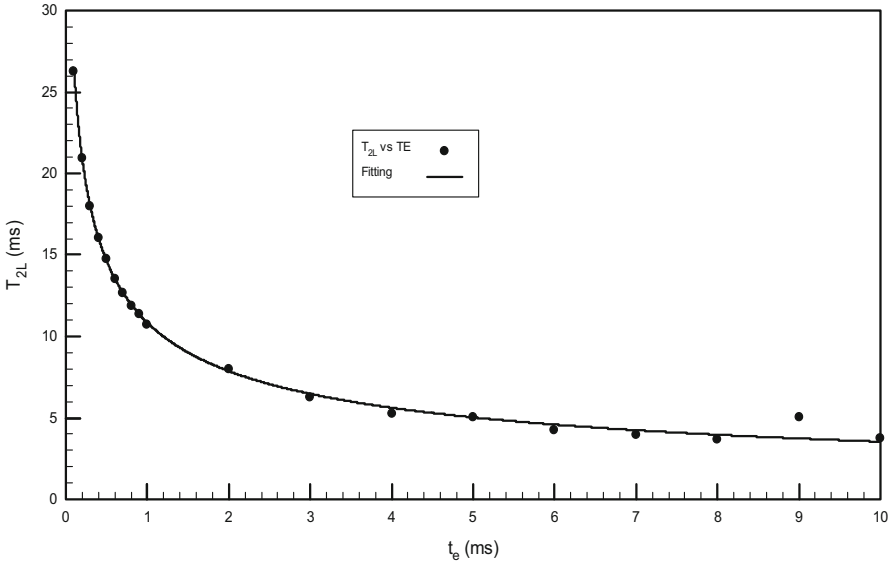

Fig. 13 T_{2L} vs. t_e, the continuous line is the fitting by Eq. (11)

Table 2 Fitting parameters corresponding to Eqs. (10) and (11)

i	β_i	a_i (μm)	G_i (Gcm^{-1})	A_i (%)
S	0.637	2.57	3176	17.55
M	0.561	9.51	556.1	53.85
L	0.515	20.13	148.1	28.6

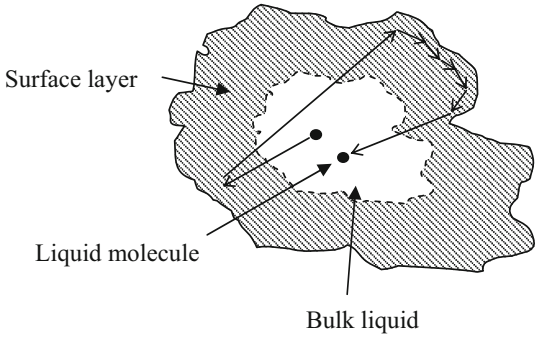

Fig. 14 Motion of a water molecule inside a pore

The obtained values of the different fitting parameters are $\rho = 0.327$ μm/ms $D = 1.86\ 10^{-9}m^2/s$, and the others are listed in Table 2.

6 Conclusions

The results show that a basic experimental method and an adequate simultaneous experimental data fitting yield excellent results to evaluate the formation characteristic of the rock as well as to provide a relaxation model. The results show that the main proton relaxation mechanisms are driven by both diffusion in the presence of internal magnetic field gradient, G, and the interaction with the surface of the pore.

The observed transversal relaxation decays are stretched exponential. This is because the complex spreading of proton relaxation processes in the pores is subject to large internal time-dependent magnetic field gradients. Some elements that contribute to this complexity are:

1. The surface of the pores is too large due to its surface tortuosity.
2. The surface diffusion is different from that in the bulk.
3. Qualitatively, the molecules residence time at the surface is greater than in the bulk (at equal effective volumes).
4. The power dependence of the relaxation at short values of both t and t_e is typical of molecules undergoing Levy walk diffusion [14, 15]. Where $0 < \beta < 1$ is the characteristic exponent of clusters undergoing a sub-diffusive dynamics. While, for ordinary diffusion, $\beta = 1$.

Figure 14 depicts the motion model of a water molecule inside a pore and the interaction with the surface tanking place in a thick layer.

Thus, the smaller the pore size, the greater the surface effect due to several sources, such as paramagnetic impurities, the tortuosity of the walls, wettability effects, and abrupt changes of magnetic susceptibility due to diffusion. Therefore, it is expected that, on average, G depends inversely on the pore size.

The use of an integrated simultaneous data fitting allows the integration of the 19 *CPMG* signals in a single adjustment in addition to a recursive fit of the relaxation times set by Eq. (11) until the dispersion is minimized. The integrated fitting required, in this case, the simultaneous determination of 80 parameters. It allowed to find that the sample possesses three types of pores characterized by their sizes, $a_S = 2.57\ \mu$m, $a_M = 9.51\ \mu$m, and $a_L = 20.13\ \mu$m with a relaxivity factor $\rho = 0.327\ \mu$m/ms, and the obtained diffusion coefficient $D = 1.86\ 10^{-9}\text{m}^2/\text{s}$ corresponds to light oil.

It has been assumed for the relaxation model that the fluid in the pore is characterized by a single diffusion coefficient. This assumption is based upon the fact that the fluids in the pores of these shale reservoirs are composed mainly of oil and small amounts of water; in addition, it is well accepted, although impossible to corroborate in this type of shale, that the water is located between the oil and the pore wall. Had we introduced two different diffusion coefficients in the dada analysis, to account for the water and oil amounts, would have introduced a mayor complexity in the data reduction.

The superposition of various stretched exponential decay curves, which takes account of different pore size sets in the sample, to describe the attenuation of the transverse magnetization is consistent with the wide variety of the data analysis of formation fluid saturated core samples. Although this method has not been developed from the basic principles, it is generally being used to describe reliably shale formations [11, 16], as described by Eqs. (10) and (11). In addition, it must be remarked that the most relevant results to be obtained are the pore sizes corresponding to the different pore sets.

Nevertheless, it should be taken into account that the standard procedure for well logging is aim to obtain a continuous pore size distribution to determine $T_{2\text{cutoff}}$ which makes sense for a porous sandstone with permeability [1]. The studied shale possesses almost no permeability, therefore, rather than a continuous pore size distribution, it is more useful to characterize the shale by the pore sizes associated with each of the different pore sets in the formation.

All the formerly show the complexity of the transversal relaxation revealed by the experimental data which is solved by the proposed model which turns out to be the most adequate to describe the experimental observation. It is also clear that these results introduce a new way to approach new studies on similar rocks and with more sophisticated *NMR* pulse sequences.

Acknowledgments This research has been fully supported Secyt-Universidad Nacional de Córdoba.

References

1. R.G. Coates, L. Xiao, M.G. Prammer, *NMR Logging, Principles and Applications* (Halliburton Energy Services, Houston, 1999)
2. A. Abragam, *The Principles of Nuclear Magnetism* (Oxford University Press, Oxford, 1961)
3. M. Mehring, *Principles of High Resolution NMR in Solids* (Springer Verlag, Berlin, 1983)
4. R.L. Kleinberg, W.E. Kenyon, P.P. Mitra, J. Magn. Reson. A **108**(2), 206 (1994)
5. C.P. Slichter, *Principles of Magnetic Resonance* (Springer Verlag, Berlin, 1990)
6. A.M. Niell, C.A. Martín, M.E. Ramia, Ann. Magn. Reson. **7**(1), 44 (2008)
7. M.D. Hürlimann, J. Magn. Reson. **148**, 367–378 (2001)
8. M.D. Hürlimann, D.D. Griffin, J. Magn. Reson. **143**, 120–135 (2000)
9. L.A. Spaletti, I. Queralt, S.D. Matheos, F. Colombo, J. Maggi, J. S. Am. Earth Sci. **25**(4), 440 (2008)
10. W.S. Price, *NMR Studies of Translational Motion* (Cambridge University Press, Cambridge, 2009)
11. M. Peyron, G.K. Pierens, A.J. Lucas, L.D. Hall, R.C. Stewart, J. Magn. Reson. A **118**, 214–220 (1996)
12. R.L. Scheaffer, T. McClave, *Probability and Statistics for Engineers*, 3rd edn. (PWS-Kent Publishing Company, Halethorpe, 1990)
13. M.E. Ramia, C.A. Martín y M.A. Chesta: Trabajos de Física, UNC—FAMAF, No 14 (2012), http://www.famaf.unc.edu.ar. Accessed 1 Apr 2012
14. T.F. Nonnenmacher, Phys. Lett. A **140**, 323 (1989)
15. H.F. Azurmendi, M.E. Ramia, J. Chem. Phys. **114**(2), 1 (2001)
16. P.P. Mitra, P. Le Doussal, Phys. Rev. B **44**, 12035 (1991)